AD-A076 128 WEAPONS SYSTEMS RESEARCH LAB ADELAIDE (AUSTRALIA) F/G 20/4
CALCULATION OF SUBSONIC NORMAL FORCE AND CENTRE OF PRESSURE POS--ETC(U)
APR 79 K D THOMSON

UNCLASSIFIED WSRL-0093-TR NL

1 OF 2
AD A 076128

END
DATE FILMED
12-79
DDC

CONT

WSRL-0093-TR

AR-001-656

(12)

LEVEL II

DEPARTMENT OF DEFENCE

DEFENCE SCIENCE AND TECHNOLOGY ORGANISATION

WEAPONS SYSTEMS RESEARCH LABORATORY

DEFENCE RESEARCH CENTRE SALISBURY
SOUTH AUSTRALIA

TECHNICAL REPORT

WSRL-0093-TR

CALCULATION OF SUBSONIC NORMAL FORCE AND CENTRE OF PRESSURE POSITION OF BODIES OF REVOLUTION USING A SLENDER BODY THEORY – BOUNDARY LAYER METHOD

K.D. THOMSON

Approved for Public Release

APRIL 1979

AR-001-656

DEPARTMENT OF DEFENCE

DEFENCE SCIENCE AND TECHNOLOGY ORGANISATION

WEAPONS SYSTEMS RESEARCH LABORATORY

(9) TECHNICAL REPORT

(14) WSRL-0093-TR

(6) CALCULATION OF SUBSONIC NORMAL FORCE AND CENTRE OF PRESSURE POSITION OF BODIES OF REVOLUTION USING A SLENDER BODY THEORY - BOUNDARY LAYER METHOD

(10) K.D. Thomson

(11) Apr 79

(12) 37

SUMMARY

The aim of this report is to present a method for predicting the aerodynamic characteristics of slender bodies of revolution at small incidence, under flow conditions such that the boundary layer is turbulent.

Firstly a panel method based on slender body theory is developed and used to calculate the surface velocity distribution on the body at zero incidence. Secondly this velocity distribution is used in conjunction with an existing boundary layer estimation method to calculate the growth of boundary layer displacement thickness which is added to the body to produce the effective aerodynamic profile. Finally, recourse is again made to slender body theory to calculate the normal force curve slope and centre of pressure position of the effective aerodynamic profile.

Comparisons made between predictions and experiment for a number of slender bodies extending from highly boattailed configurations to ogive-cylinders, and covering a large range of boundary layer growth rates, indicate that the method is useful for missile design purposes.

POSTAL ADDRESS: Chief Superintendent, Weapons Systems Research Laboratory, Box 2151, G.P.O., Adelaide, South Australia, 5001.

DOCUMENT CONTROL DATA SHEET

Security classification of this page: UNCLASSIFIED

1 DOCUMENT NUMBERS	
AR Number:	AR-001-656
Report Number:	WSRL-0093-TR
Other Numbers:	

2 SECURITY CLASSIFICATION	
a. Complete Document:	Unclassified
b. Title in Isolation:	Unclassified
c. Summary in Isolation:	Unclassified

3 TITLE: CALCULATION OF SUBSONIC NORMAL FORCE AND CENTRE OF PRESSURE POSITION OF BODIES OF REVOLUTION USING A SLENDER BODY THEORY - BOUNDARY LAYER METHOD.

4 PERSONAL AUTHOR(S):

K.D. Thomson

5 DOCUMENT DATE: April 1979

6 6.1 TOTAL NUMBER OF PAGES: 32

6.2 NUMBER OF REFERENCES: 20

7 7.1 CORPORATE AUTHOR(S):

Weapons Systems Research Laboratory

7.2 DOCUMENT SERIES AND NUMBER

Weapons Systems Research Laboratory 0093-TR

8 REFERENCE NUMBERS

a. Task: DST 76/118

b. Sponsoring Agency:

9 COST CODE:

10 IMPRINT (Publishing organisation)

Defence Research Centre Salisbury

11 COMPUTER PROGRAM(S) (Title(s) and language(s))

12 RELEASE LIMITATIONS (of the document):

Approved for Public Release

12.0	OVERSEAS	NO		P.R.	1	A		B		C		D		E	

Security classification of this page: UNCLASSIFIED

Security classification of this page: UNCLASSIFIED

13 ANNOUNCEMENT LIMITATIONS (of the information on these pages):

No limitation

14 DESCRIPTORS:

a. EJC Thesaurus Terms

Bodies of revolution
Slender bodies
Boundary layer
Aerodynamic characteristics
Missiles
Missile airframes
Aerodynamic configurations
Ogives
Cylindrical bodies

b. Non-Thesaurus Terms

15 COSATI CODES:

0103

16 LIBRARY LOCATION CODES (for libraries listed in the distribution):

17 SUMMARY OR ABSTRACT:
(if this is security classified, the announcement of this report will be similarly classified)

The aim of this report is to present a method for predicting the aerodynamic characteristics of slender bodies of revolution at small incidence, under flow conditions such that the boundary layer is turbulent.

Firstly, a panel method based on slender body theory is developed and used to calculate the surface velocity distribution on the body at zero incidence. Secondly, this velocity distribution is used in conjunction with an existing boundary layer estimation method to calculate the growth of boundary layer displacement thickness which is added to the body to produce the effective aerodynamic profile. Finally, recourse is again made to slender body theory to calculate the normal force curve slope and centre of pressure position of the effective aerodynamic profile.

Comparisons made between predictions and experiment for a number of slender bodies extending from highly boattailed configurations to ogive-cylinders, and covering a large range of boundary layer growth rates, indicate that the method is useful for missile design purposes.

Security classification of this page: UNCLASSIFIED

TABLE OF CONTENTS

	Page No.
1. INTRODUCTION	1 - 2
2. VELOCITY DISTRIBUTION	2 - 3
3. BOUNDARY LAYER DEVELOPMENT	5 - 7
4. EXAMPLES	7 - 14
4.1 Slender boattailed bodies	7 - 10
4.1.1 Body no. 1	7 - 9
4.1.2 Body no. 2	9 - 10
4.2 Non-slender boattailed bodies	10
4.3 Ogive-cylinders	10 - 13
4.4 Shell configuration	13 - 14
5. CONCLUDING REMARKS	14
6. ACKNOWLEDGEMENT	15
NOTATION	16 - 17
REFERENCES	18 - 19

LIST OF FIGURES

1. Types of S"(x) distribution considered	4
2. Approximation to body no. 1 and calculated velocity distribution at $M_o = 0$, $\alpha = 0^o$	8
3. Approximation to body no. 2	9
4. Approximation to bodies no. 3 and 4 and calculated velocity distributions at $M_o = 0$, $\alpha = 0^o$	11
5. Approximation to body no. 5	12
6. Approximation to body no. 6	12
7. Approximation to body no. 7	13
8. Body component parts	23
9. Comparison between nose profiles of bodies 1 to 7 and profile produced by chosen S"(x) distribution	25
TABLE 1. COMPARISON OF MEASURED AND ESTIMATED NORMAL FORCE CURVE SLOPE AND CENTRE OF PRESSURE POSITION FOR MISSILE BODIES	20
APPENDIX I EVALUATION OF PERTURBATION VELOCITIES ASSOCIATED WITH NOSES, BOATTAILS AND STABILISING FLARES	21 - 27

1. INTRODUCTION

Calculations based on potential flow aerodynamic theories generally provide reasonably close approximations to the lift and pitching moment experienced by near-planar configurations such as aerofoils and wings at small angles of incidence. However, similar calculations applied to extreme three-dimensional shapes such as bodies of revolution often lead to force and moment estimates which are grossly in error, particularly if the body has a boattail. The main source of error is that potential flow methods do not admit the development of a boundary layer, which, at the Reynolds numbers of practical interest, is predominantly turbulent. For an aerofoil or wing the boundary layer displacement thickness provides a thin sheath about the wing surface, and this causes a small perturbation to lift and pitching moment. Wing lift calculations are often refined by allowing for the displacement thickness of the boundary layer as an additional contribution to the aerofoil thickness distribution. For a body of revolution at small incidence the boundary layer thickness can grow very rapidly (particularly if the body has a boattail, in which case the pressure gradient is adverse over the rear of the body, and at the same time the streamlines are converging) and the displacement thickness of the boundary layer envelops the body in a sheath which produces a substantially changed aerodynamic profile, with consequent large changes in aerodynamic properties.

This feature can be readily illustrated using the results of slender body theory. Thus (see, for example, Ward (1)) the normal force (-Z) and pitching moment (M) about the nose on a slender body of revolution with pointed nose and incidence α, are given by

$$\left.\begin{aligned} -Z &= \rho U_0^2 \alpha\, S(L) \\ \text{and} \qquad M &= -\rho U_0^2\, \alpha \,\{\, LS(L) - V\}\ , \end{aligned}\right\} \tag{1}$$

where L is the body length,

S(L) is the base cross-sectional area,

U_0 is the free stream speed,

V is the volume of the body, and

ρ is the fluid density.

When the body has a boattail, S(L) can be much less than the maximum cross-sectional area, and equation (1) shows that Z will then be small and M is likely to be positive. If slender body theory is applied to the profile formed by the addition of the boundary layer sheath (the displacement thickness) to the body profile, then the effective base area will be substantially greater than S(L) and V will be increased. The net effect is to cause a substantial increase in normal force (perhaps by a factor of 2) and in most cases a very much less positive pitching moment. The effect of the boundary layer displacement thickness is thus seen to be very significant, and should be included in aerodynamic estimates, particularly when boattailed bodies are being examined.

This is not a new idea and has been in vogue for some decades. For example, it was used by Young (2) and Myring (3) in estimating the drag of bodies of revolution, while its use is basic to theoretical estimates of the Magnus force and moment experienced by slender rotating bodies of revolution (see for example, references 4 to 7). Recently, Esch (8) included the boundary layer displacement thickness in his comprehensive investigation into the effects of Reynolds number and transition position on the normal force and pitching moment characteristics of long slender ogive-cylinders.

The aim of the present study has been to develop a method of calculating the normal force and centre of pressure position of bodies of revolution at subsonic speeds and low incidence, covering all slender shapes irrespective of whether they have boattails or not. Simplicity has been a prime consideration in the development of each step of the method, even at the expense of some loss in accuracy. At the outset it is stated that a universal, accurate, simple method was not achieved, but, provided that the body is reasonably slender, estimates are obtained which are adequate for many design purposes.

The method is divided into three parts. First the inviscid-flow velocity distribution on the body surface is calculated; then the distribution of boundary layer displacement thickness, which defines the aerodynamic sheath surrounding the body and thus the effective aerodynamic profile; and finally the normal force and centre of pressure position are calculated by applying slender body theory to the effective aerodynamic profile. In Section 2 a panel method based on slender body theory is outlined (and developed in Appendix I) to enable calculation of the velocity distribution. The turbulent boundary layer method of Stratford and Beavers (9) is adapted in Section 3 for calculating the displacement thickness, while in Section 4 these methods are applied to a number of configurations, and the estimated normal force characteristics and centre of pressure positions are compared with experimentally determined values.

2. VELOCITY DISTRIBUTION

The pressure gradients over the nose and the downstream parallel section of a body of revolution are such that the boundary layer growth rate is small. In these regions the aerodynamic profile is therefore little different in shape from the body profile, and errors in calculated boundary layer thickness distribution arising from errors in surface velocity distribution are unimportant. Hence over the nose and parallel section some simplifying approximations can be used in calculating the velocity distribution. In the vicinity of the boattail the boundary layer grows very rapidly, due to the combined effect of an adverse pressure gradient and also to the convergence of streamlines, which provides a mechanism by which the thickening boundary layer is concentrated and thus thickens further. It will be demonstrated in Section 4 that even here some errors in velocity distribution can be tolerated. It appears that the rate of boundary layer growth caused by streamline convergence is so significant that, in comparison, errors introduced by moderate inaccuracies in the representation of velocity gradient are relatively unimportant.

Hence, summing up, the boundary layer behaviour over all sections of the body can be adequately predicted using an approximate representation to the velocity distribution.

As discussed in Section 3 the boundary layer displacement thickness distribution is calculated at zero incidence only and is added to the body to find an effective aerodynamic profile which is taken to hold for all (small) incidences. It is therefore only necessary to calculate the velocity distribution at zero incidence, and the method selected is based on an application of slender body theory by Spreiter and Alksne (10), who derived an expression particularly suitable for this purpose. Thus, considering the uniform flow at speed U_0 over a smooth pointed slender body of revolution at zero incidence, the perturbation velocity u is given by

$$\frac{u}{U_0} = \frac{S''(x)}{2\pi} \ln \frac{\beta r}{2\sqrt{x(L-x)}} - \frac{1}{4\pi}\int_0^L \frac{[S''(\xi)-S''(x)]}{|x-\xi|}d\xi \,, \qquad (2)$$

where L is the body length,

S is the body cross-sectional area distribution,

$S''(x) = \frac{d^2S}{dx^2}$,

x is the axial coordinate measured from the origin at the nose,

r is the body radius at station x,

$\beta = \sqrt{1-M_0^2}$, M_0 being the freestream Mach number,

and ξ is a dummy variable.

Equation (2) becomes particularly simple to evaluate if the S'' terms are either constant or vary linearly with x. Now, most missile body configurations are composed of a conical or ogival nose, one or more parallel sections, and perhaps a boattail or flare. S''(x) is constant for a conical nose, a boattail and a flare, and is zero for a parallel section. Furthermore, a linear distribution of S''(x) of the form S''(x) = ax +b may be shown (see Appendix I) to represent a curved nose profile which, in the context of this investigation, can be taken as an approximate representation of all ogival nose profiles. Hence, various sections of a body of revolution can be considered as panels, in each of which S''(x) is either constant or varies linearly. If equation (2) is solved for these cases the total perturbation velocity can be found by summing together the contributions produced by the individual panels. It will be appreciated that the representation of a body by a number of panels in the manner described above is likely to lead to a discontinuous distribution of S''(x). At each discontinuity slender body theory breaks down and indicates a singular behaviour in the perturbation velocity. However, it usually happens that S''(x) discontinuities are located sufficiently far apart for the regions of singular behaviour to be reasonably separated, and they can be smoothed out and still permit an adequate prediction of the velocity distribution. Examples to be given in Section 4 will illustrate this point.

The three S''(x) distributions illustrated in figure 1 require examination and the appropriate perturbation velocities are evaluated in Appendix 1, which also includes the application of S''(x) distributions to noses, boattails and stabilising flares.

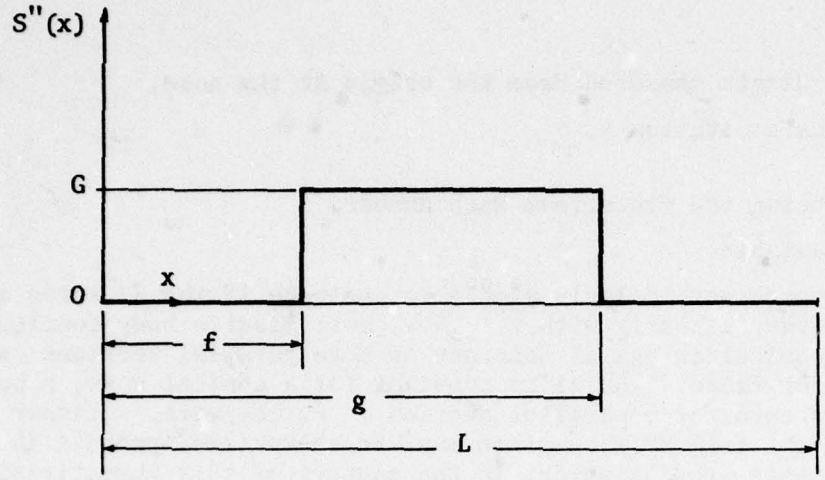

(a) Rectangular distribution

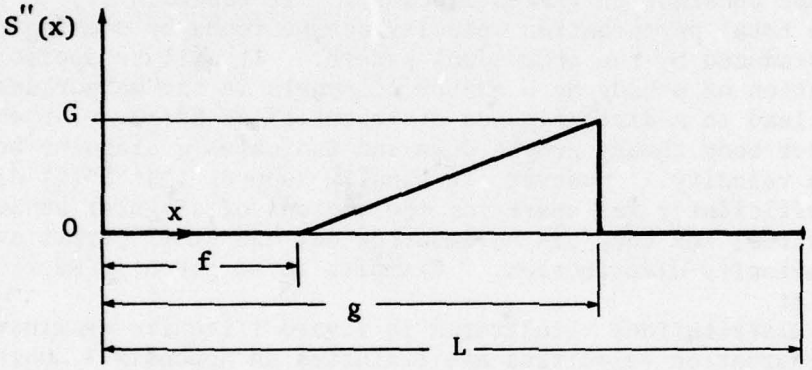

(b) Triangular distribution - increasing with x

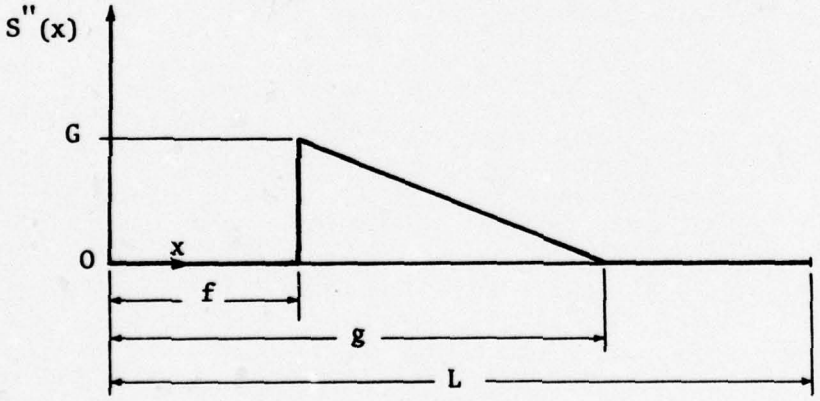

(c) Triangular distribution - decreasing with x

Figure 1. Types of S"(x) distribution considered

3. BOUNDARY LAYER DEVELOPMENT

When a body of revolution is at incidence a different boundary layer displacement thickness distribution develops along each meridian, and the effective aerodynamic body will not be a body of revolution. If, as mentioned in Section 1, this meridianal variation is ignored and the boundary layer growth is calculated at zero incidence only, the method of approach is kept simple, but at the expense of some loss in accuracy. In an endeavour to estimate the magnitude of this loss an investigation was conducted in which for one slender boattailed body (body no. 1) the velocity distribution was calculated on the extreme windward and leeward meridians at 5^{o} incidence. The boundary layer displacement thickness distributions were then estimated and were found to differ considerably, their mean being close to the distribution calculated on the body in axisymmetric flow. However, in this report the effective aerodynamic profiles rather than boundary layer thickness distributions should be compared. Such a comparison revealed a small relative difference between the effective aerodynamic profiles at 5^{o} and at 0^{o} incidence.

A further effect of different boundary layer growth rates on the windward and leeward sides is that the effective aerodynamic profile is not symmetrical but has a curved centreline, which of course influences the aerodynamic loading. For the particular case investigated above the non-uniform boundary layer growth yielded an effective aerodynamic boattail with an incidence about 3% less than the geometrical value, which was calculated (using an application of slender body theory reported by Isaacs (11)) to give a 5% increase in normal force curve slope and a forward centre of pressure movement of less than 0.3 calibres. Although these increments are significant (particularly that to normal force curve slope) the method proposed does not include an allowance specifically to cover boundary layer induced camber. The boundary layer displacement thickness distribution on the body at zero incidence is calculated and added to the body to find an effective aerodynamic profile that is taken to hold for all (small) incidences. As will be described shortly an empirically determined value of the boundary layer shape factor is used in the boattail region to enable calculation of the displacement thickness there. The choice of shape factor is such that in most cases the error in estimated normal force curve slope is considerably less than 5%.

Stratford and Beavers (9) formulated a convenient method for calculating the turbulent boundary layer properties of two and three-dimensional shapes in compressible flow. At any point the boundary layer is represented as that growing on an equivalent flat plate at a distance from the leading edge dependent upon surface Mach number distribution and body shape. Now, slender body theory shows that compressibility effects are not very pronounced for slender bodies of revolution (as shown by the weak influence of the terms in β in equations (I.1) (I.2) and (I.3) and therefore an incompressible version of Stratford and Beavers' method is considered. Thus, the boundary layer at distance x from the body nose is the same as that on a flat plate at distance X from the leading edge given by

$$X = \left[\left(\frac{U}{U_0}\right)^4 r^{\gamma}\right]^{-1} \int_0^x \left(\frac{U}{U_0}\right)^4 r^{\gamma}\, dx \ ,$$

where U is the fluid speed at the body surface,

γ is a constant such that

$\gamma = 1.25$ when $R_X \sim 10^6$,

$\gamma = 1.20$ when $R_X \sim 10^7$,

and $R_X = \frac{UX}{\nu}$

is a Reynolds number based on local stream speed outside the boundary layer, ν being the kinematic viscosity.

The momentum thickness θ is given by

$$\left.\begin{aligned} \theta &= 0.036 \text{ X } R_X^{-\frac{1}{5}} \quad \text{for } R_X \sim 10^6 \text{ ,} \\ \theta &= 0.022 \text{ X } R_X^{-\frac{1}{6}} \quad \text{for } R_X \sim 10^7 \text{ .} \end{aligned}\right\} \tag{3}$$

Stratford and Beavers recommend determination of the displacement thickness δ^* for small pressure gradients by assuming a 1/7th power law velocity profile, from which the shape factor $H = \frac{\delta^*}{\theta}$ can be evaluated and thence δ^* using equation (3). Thus,

$$\left.\begin{aligned} \delta^* &= 0.036 \text{ HXR}_X^{-\frac{1}{5}} \quad \text{for } R_X \sim 10^6 \text{ ,} \\ \delta^* &= 0.022 \text{ HXR}_X^{-\frac{1}{6}} \quad \text{for } R_X \sim 10^7 \text{ ,} \end{aligned}\right\} \tag{4}$$

For severe pressure gradients, Stratford and Beavers recommend calculating the variation of H over the body surface, and thence δ^* from (4). The method adopted in this report is to treat the body in two sections, namely that part over which the cross-sectional area (or radius) increases with axial distance or is constant, and that part over which it decreases with axial distance (i.e., the boattail section). Over the first part the boundary layer growth is generally similar to that over a flat plate, for which the commonly accepted value of H = 1.4 is used. Over a boattail the pressure gradient can be very severe indeed and H will increase substantially beyond 1.4. Reference 12 contains several sets of experimental data relevant to the flow over bodies, and examples* roughly representative of boattail flows give values of H between 2 and 4.

To simplify boundary layer calculations over the boattail, the variation of H with axial distance from 1.4 to perhaps greater than 3 has been replaced by a constant value for all boattails, chosen empirically using the following approach. Equation (1) shows that the body normal force depends on the base area S(L) of the effective aerodynamic profile, and that S(L) is also a dominant parameter in determining the pitching moment and therefore the centre of pressure position.

Now $$S(L) = \pi \left(r_B + \delta_B^* \right)^2 = \pi r_B^2 \left(1 + \frac{\delta_B^*}{r_B} \right)^2 \text{ ,}$$

where subscript B refers to conditions at the base. Any errors in δ_B^* will be of greatest significance on configurations for which r_B is small, i.e., on body shapes with extensive boattailing. It follows that if H is chosen empirically it should be selected in such a way that the predicted and measured normal force and centre of pressure positions match as closely as possible for bodies with extensive boattails, since these are the key configurations. If this chosen H is then applied to evaluate δ^* on a body with less severe boattailing, it will overestimate δ_B^*, but because r_B is now not so small the errors in S(L)

* Relevant examples are those numbered 3600, 3700, 3800, 4000, 5000 and 5100 in reference 12.

(and therefore in normal force and pitching moment) are not likely to be very significant. Thus, a single H value can be chosen to cover all boattails. By examining several boattailed bodies it was found that H = 3.0 led to the best overall estimate of normal force and centre of pressure position for boattailed bodies.

Summing up, over that part of a body where the radius either increases with axial distance or is constant, H is taken to be 1.4. When the radius decreases with axial distance H is taken to be 3.0. The appropriate value of H is substituted into equation (4) for the evaluation of δ^*.

This simple choice of two constant values for H can lead to an uncertainty when considering a configuration with a parallel afterbody. Thus, the afterbody can be thought of either as a section having constant radius, in which case H = 1.4, or as the limiting case for a boattail, namely a zero-angle boattail, in which case H = 3.0. These two alternatives have been examined in Section 4 in connection with two ogive-cylinders (bodies no. 5 and 6), and the differences were found to be small. This finding is consistent with the statement made above that for such bodies $\frac{\delta_B^*}{r_B}$ is small and changes due to errors in estimates of δ_B^* are not likely to be very significant.

It will be noted that since H changes its value discontinuously at the junction of a parallel section and a boattail, δ^* will change discontinuously there and the effective aerodynamic profile will also have a discontinuity. This reflects the crudeness of the method in replacing a varying shape factor over the boattail by a constant value. Even though slender body theory does not hold in the vicinity of this discontinuity, nevertheless equation (1) can be applied to evaluate both normal force and pitching moment and thence the centre of pressure position of the effective aerodynamic profile.

4. EXAMPLES

Several examples are given below in order to illustrate how well the surface velocity distribution can be predicted by remarkably few panels of either constant or linearly varying S"(x), and also how closely the method predicts the normal force and centre of pressure position. Although experimental normal force and centre of pressure position data are presented at speeds high enough for the effects of compressibility to be experienced, in the interests of simplicity all velocity distributions and boundary layer calculations have been based on incompressible flow considerations.

4.1 Slender boattailed bodies

4.1.1 Body no. 1

The slender bomb body configuration (figure 2(a)) was represented by five panels of S"(x) distribution, as shown in figure 2(b). The curved nose was represented by the "universal" nose profile (equation (I-4)) and the corresponding S"(x) distributions comprising two panels, the boattail by a single panel having a constant S"(x) distribution, and two panels representing the curved transition region between the parallel centre section and the boattail. The crosses in figure 2(a) show the profile produced by these panels and the agreement with the actual profile is seen to be close. The deduced velocity distribution is given in figure 2(c). Also shown in this figure is a velocity distribution calculated by Haselgrove (13) who adapted a computer programme of Albone (14), results of which are highly accurate for slender shapes. Apart from singular regions occurring at the beginning and end of S"(x) distributions, the two velocity distributions agree closely. Furthermore, except near the nose point, the most obvious line through the singular regions provides a close estimate of the velocity distribution.

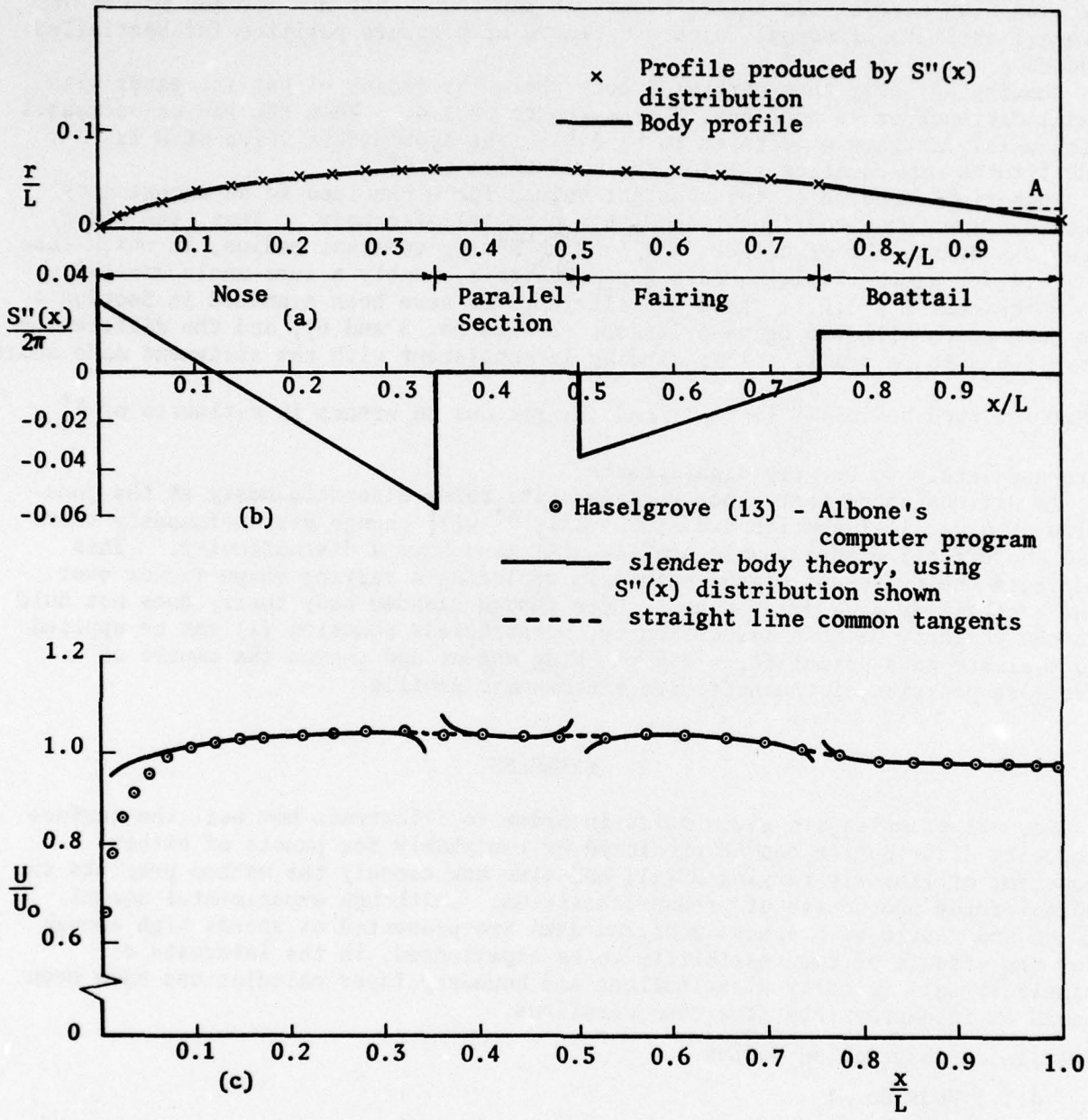

Figure 2. Approximation to body no. 1 and calculated velocity distribution at $M_o = 0$, $\alpha = 0^o$

(a) Body profile

(b) S"(x) distribution

(c) Velocity distribution

The discrepancy near the nose point is significant but it will not lead to large errors in estimates of boundary layer displacement thickness distribution because of the highly favourable pressure gradient and the expanding body surface with axial distance, both of which lead to a thin boundary layer. The comparison in figure 2(c) provides an indication that, at zero incidence at least, the body in figure 2(a) behaves as if slender everywhere except near the nose.

The shape in figure 2(a) was tested in a wind tunnel by Landers (15) who, in order to allow for an internal strain gauge force measurement balance, had to distort the rear of the body as shown in the region A in figure 2(a). In these experiments Landers used a nose boundary layer trip to ensure that a turbulent boundary layer occurred; he also checked that the flow was attached over the boattail. The experimental results of normal force coefficient slope and centre of pressure position are given in Table 1. Also shown are the results of slender body theory assuming inviscid flow, and in addition the estimated values based on the method of this paper, using the velocity distribution in figure 2(c). For both of these estimates, allowance was made for the base distortion shown in figure 2(a). The present method is seen to provide a large correction to slender body theory and to predict normal force and centre of pressure characteristics which are in reasonably close agreement with experiment.

4.1.2 Body no. 2

The body profile in figure 3(a) was represented approximately by four panels (figure 3(b)), two representing the nose and two the boattail. The profile thus produced is seen to match the body closely except for the front half of the nose which is too fat.

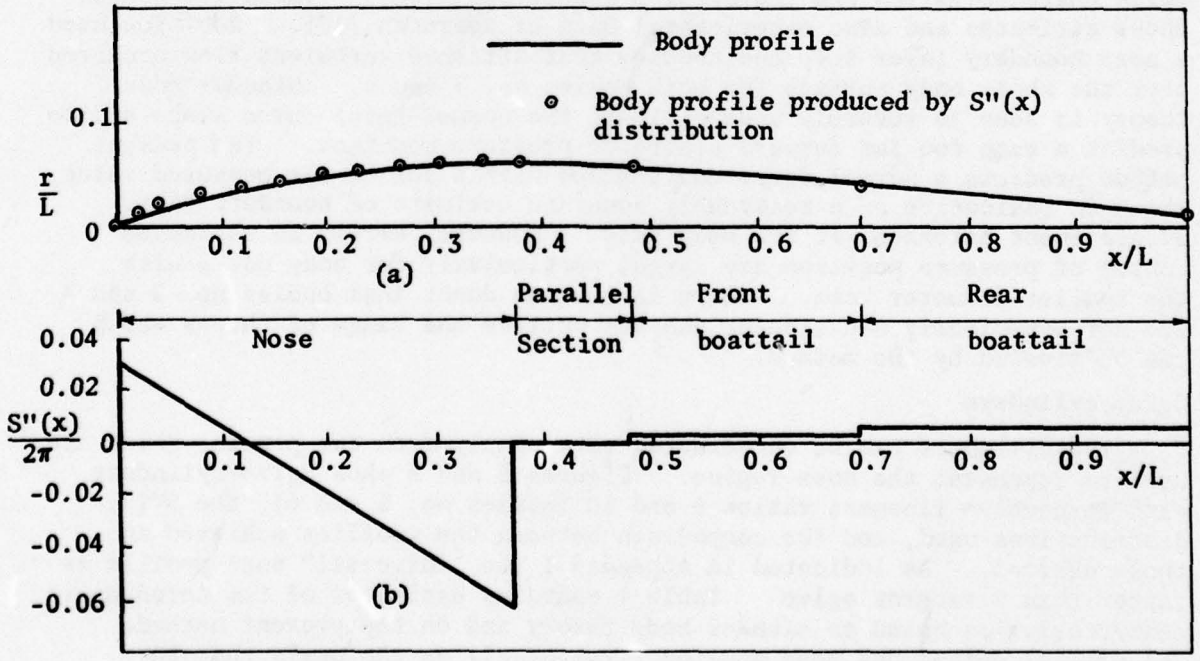

(a) Body profile

(b) S"(x) distribution

Figure 3. Approximation to body no. 2

Calculated slender body characteristics and those given by the present method are shown at the second entry in Table 1, where they are compared with the measurements of Marsden (16) made at high Reynolds number. Again the defects of slender body theory in inviscid flow are revealed, as well as the gratifying agreement produced by the present method.

4.2 Non-slender boattailed bodies

The next two examples concerning the two bodies shown in figure 4 are interesting in that they indicate what might happen when the method is applied to configurations which do not satisfy the slenderness requirements of slender body theory. Both bodies have the same blunt nose and a relatively steep boattail angle. Body no. 3 boattail extends to the base while no. 4 has a parallel afterbody. A close match to both shapes was achieved by using two panels to represent the nose and one to represent the boattail (S"(x) distribution A in figure 4(b)). In addition, further panels were also used to fair the sharp kinks in body profile at either end of the boattail, thus weakening the singularities in their vicinity. The velocity distributions calculated from the panels are shown in figure 4(c) which also contains a much more accurate velocity distribution calculated by Haselgrove (13). In spite of the close match to the body profiles illustrated in figure 4(a), slender body theory produces substantial errors in velocity distribution, particularly in the vicinity of the nose. The addition of extra panels to reduce singular behaviour at either end of the boattail is seen to produce significant improvements in velocity distribution. Even so, the singular regions are still extensive and substantial smoothing is required, the use of straight line common tangents being a useful artifice. However, the smoothed velocity distribution does bear some resemblance to Haselgrove's velocity distribution. The strength of the singularities associated with this configuration gives a pointer that the application of slender body theory to the effective aerodynamic profile is likely to produce errors in normal force characteristics and centre of pressure positions. Table 1 contains these estimates and also experimental data of Robinson (17). Robinson used a nose boundary layer trip and checked that attached turbulent flow occurred over the whole body surface for both bodies no. 3 and 4. Slender body theory is seen to severely underestimate the normal force curve slope and to predict a much too far forward centre of pressure position. The present method predicts a normal force curve slope within 10% of the measured value, which is indicative of a reasonably accurate estimate of boundary layer displacement thickness at the body base. However, errors in estimated centre of pressure position are large, particularly for body no. 3 with the smaller diameter base. There is thus no doubt that bodies no. 3 and 4 are aerodynamically non-slender and lie outside the range of shapes which can be treated by the method.

4.3 Ogive-cylinders

Ogive-cylinders can be constructed very simply from two panels, which are used to represent the nose region. Figures 5 and 6 show ogive-cylinders with respective fineness ratios 6 and 10 (bodies no. 5 and 6), the S"(x) distributions used, and the comparison between the profiles achieved and those desired. As indicated in Appendix I the "universal" nose profile is fatter than a tangent ogive. Table 1 contains estimates of the aerodynamic characteristics based on slender body theory and on the present method. The present method has been applied first of all on the basis that the parallel afterbody is a cylindrical section, for which the boundary layer shape factor is 1.4, and secondly, by treating the rear half of the afterbody as the extreme case of a boattail of zero angle, over which, by the empiricism in Section 3, $H = 3.0$.

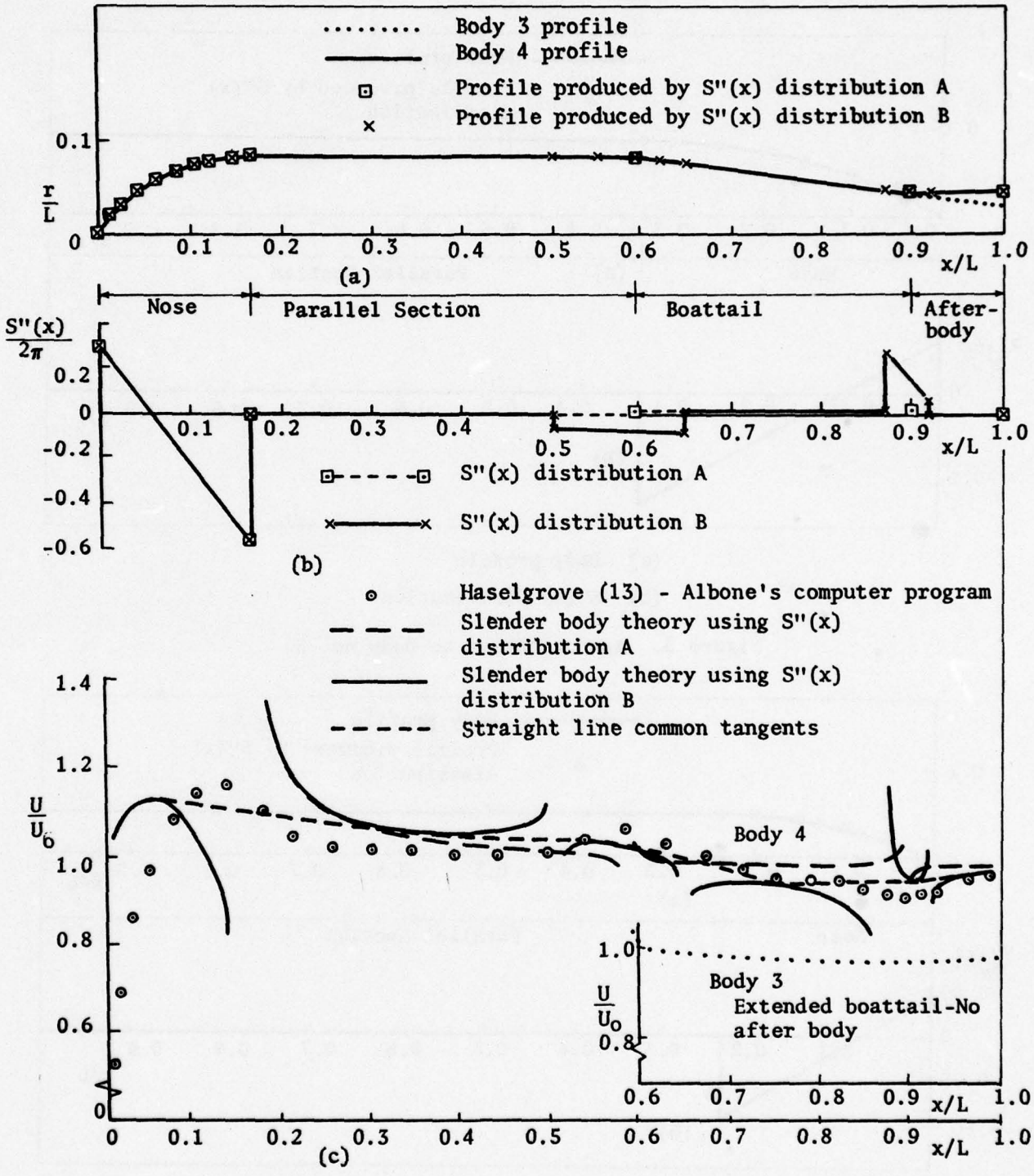

(a) Body profiles

(b) S"(x) distributions for body no. 3

(c) Velocity distributions

Figure 4. Approximation to bodies no. 3 and 4 and calculated velocity distributions at $M_o = 0$, $\alpha = 0^o$

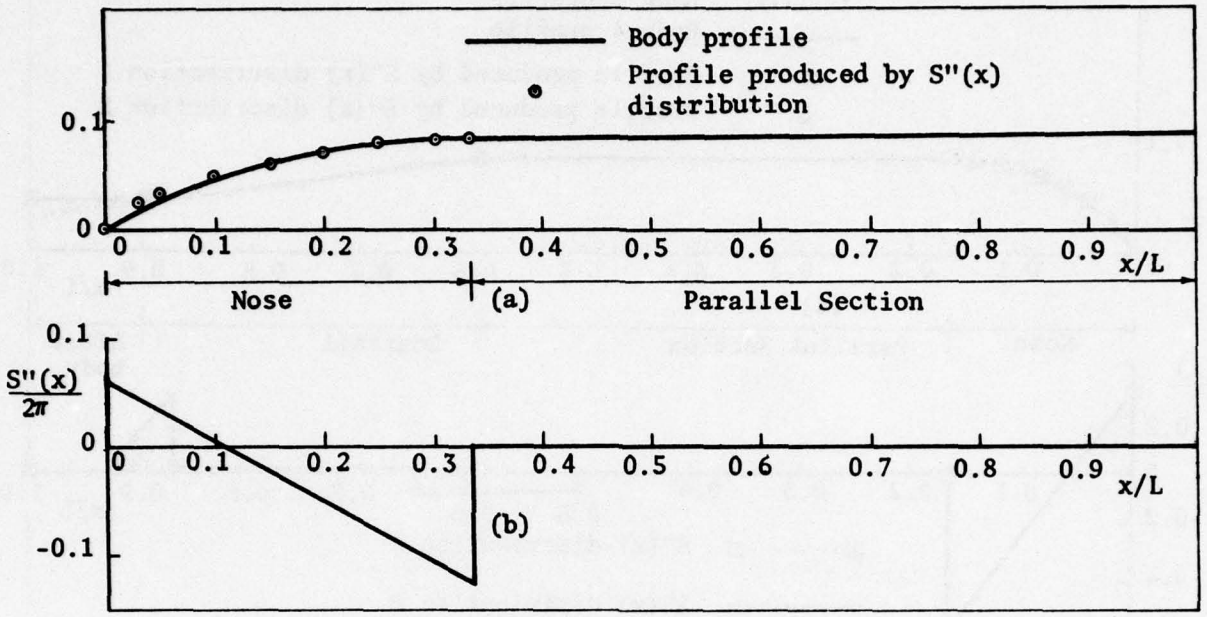

(a) Body profile

(b) S"(x) distribution

Figure 5. Approximation to body no. 5

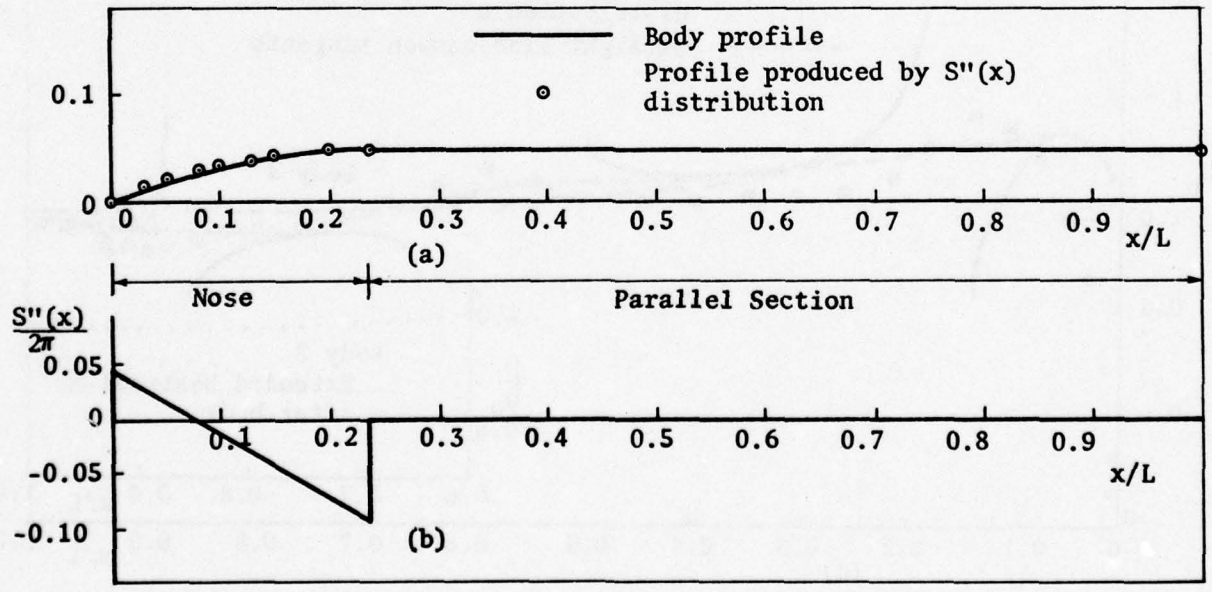

(a) Body profile

(b) S"(x) distribution

Figure 6. Approximation to body no. 6

The estimates for body no. 5 are compared with normal force data taken from experiments by Ward (18) and an empirically determined centre of pressure position given by Darling (19). Comparative data for body no. 6 were obtained by Robinson (17), who used a nose boundary layer trip to ensure the development of a turbulent boundary layer. For both these shapes the boundary layer displacement thickness is small compared with the base radius and slender body theory gives close estimates of normal force curve slope and centre of pressure position. Allowing for the boundary layer growth by using the present method gives excellent agreement with experiment. As mentioned in Section 3, the small changes resulting from treating the afterbody as a cylinder or as a zero-angle boattail are unimportant.

4.4 Shell configuration

The nose bluntness of body no. 7 in figure 7(a) was ignored and the body represented by two panels in the nose region and one over the boattail (figure 7(b). The final entry in Table 1 shows a comparison between results of slender body theory, the present method, and experimental data of Jermey (20).

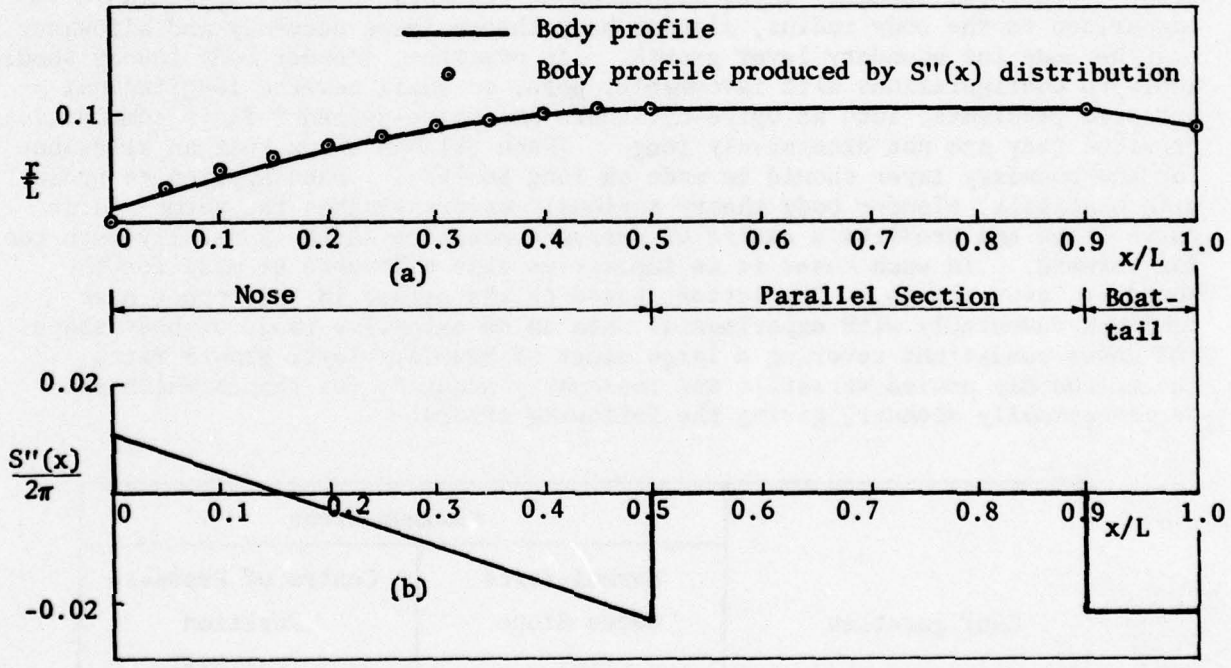

(a) Body profile

(b) S"(x) distribution

Figure 7. Approximation to body no. 7

Jermey's experiments were at moderately low Reynolds number and he forced boundary layer transition on the nose by a boundary layer trip. Slender body theory is seen to underestimate normal force curve slope and to predict the centre of pressure position too far forward, whereas results using the present method compare closely with experiment.

5. CONCLUDING REMARKS

The success or otherwise of the present method appears to depend largely on whether the body being examined is aerodynamically slender. Slender body theory defines what this means mathematically but does not give a quantitative explanation. Criteria defining the limits of aerodynamic slenderness are needed but none are offered in this report. Of the cases that have been examined, bodies no. 3 and 4 are not aerodynamically slender, particularly in the vicinity of the nose, whereas, generally speaking the other bodies are. In any case where the body is aerodynamically slender and the boundary layer displacement thickness is everywhere small relative to the body radius, slender body theory can be used to give close estimates of normal force and centre of pressure position. Where the boundary layer displacement thickness becomes appreciable in comparison to the body radius, slender body theory loses accuracy and allowance must be made for boundary layer growth. In practice, slender body theory should apply to configurations with favourable, zero, or small adverse longitudinal pressure gradients, such as ogive-cylinders and ogive-cylinder-flare combinations, provided they are not excessively long. (Esch (8) has shown that an allowance for the boundary layer should be made on long bodies). When applied to bodies with boattails, slender body theory seriously underestimates the normal force curve slope and predicts a centre of pressure position which is usually much too far forward. In such cases it is imperative that allowance be made for the boundary layer growth. Predictions based on the method in this paper have compared favourably with experimental data on an extensive range of body shapes and under conditions covering a large range of boundary layer growth rates. The method has proved versatile and reasonably accurate for shapes which are aerodynamically slender, giving the following errors:

Configuration	Maximum Error	
	Normal force Curve Slope (%)	Centre of Pressure Position (Calibre)
Bodies without extensive boattails	5	0.6
Bodies with extensive boattails	3	2.2

Increased accuracy could probably be achieved by allowing for boundary layer induced camber and making a suitable compensating adjustment to the value of the boundary layer shape factor in regions of adverse pressure gradient, but at the cost of increased complexity.

6. ACKNOWLEDGEMENT

Acknowledgement is made to the advice and assistance of Mr L.M. Sheppard, who pointed out that Spreiter and Alksne (10) had derived equation (2), on which the method of estimating the velocity distribution is based.

NOTATION

G	maximum value of S"(x)
H	boundary layer shape factor (= $\frac{\delta^*}{\theta}$)
J	parameter related to boattail angle
L	body length
L_N	nose length
M	pitching moment about nose
M_o	free stream Mach number
R_X	a Reynolds no. (= $\frac{UX}{\nu}$)
S(x)	body cross-sectional area at station x
S(L)	cross-sectional area at body base
S"(x)	= $\frac{d^2S}{dx^2}$
U_o	free stream speed
U	fluid speed at edge of boundary layer
V	body volume
X	distance from leading edge of equivalent flat plate
Z	minus normal force
a,b,c,d	constants in polynominal equation
f,g	lengths defined in figure 1
r	body radius
r_o	body radius at end of nose section
u	perturbation velocity
x	axial coordinate
α	body incidence
β	= $\sqrt{1-M_o^2}$
γ	a constant, whose value depends on the magnitude of R_X
δ^*	boundary layer displacement thickness

θ	boundary layer momentum thickness
ν	kinematic viscosity
ξ	a dummy variable
ρ	fluid density
	subscripts
1,2,3	locations of changes in body shape (figure 8)
B	body base

REFERENCES

No.	Author	Title
1	Ward, G.N.	"Linearised Theory of Steady High Speed Flow". 1 st ed. Ch. 9. Cambridge Univeristy Press, 1955
2	Young, A.D.	"The Calculation of the Total and Skin Friction Drags of Bodies of Revolution at Zero Incidence". ARC R&M 1874, 1939
3	Myring, D.F.	"The Profile Drag of Bodies of Revolution in Subsonic Axisymmetric Flow". RAE Tech Report 72234, 1973
4	Martin, J.C.	"On Magnus Effects Caused by the Boundary Layer Displacement Thickness on Bodies of Revolution at Small Angles of Attack". BRL Report 870, 1955
5	Kelly, H.R. and Thacker, R.G.	"The Effect of High Spin on the Magnus Force on a Cylinder at Small Angles of Attack". NAVORD Report 5036, 1956
6	Sedney, R.	"Laminar Boundary Layer on a Spinning Cone at Small Angles of Attack". BRL Report 991, 1956
7	Vaughn, H.R. and Reis, G.E.	"A Magnus Theory". AIAA Journal, Vol. 11, No. 10, October, 1973
8	Esch, H.	"Der Einfluss Der Reynoldszahl Auf Die Normalkraftcharakteristik Schlanker Zylindrischer Rümpfe". ZLR Report 75-09, 1975
9	Stratford, B.S. and Beavers, G.S.	"The Calculation of the Compressible Turbulent Boundary Layer in an Arbitrary Pressure Gradient - A Correlation of Certain Previous Methods". ARC R&M 3207, 1961
10	Spreiter, J.R. and Alksne, A.Y.	"Slender-body Theory Based on Approximate Solution of the Transonic Flow Equation". NASA Tech Report R-2, 1959
11	Isaacs, D.	"The Use of Slender Body and Linear Theory for Calculating the Loading on Axisymmetric Bodies in Non-Uniform Subcritical Flow". Proceedings of Fourth Meeting of TTCP Technical Panel W-2, held in Australia, November, 1977, p. 85

No.	Author	Title
12	Coles, D.E. and Hirst, E.A. (Editors)	Proceedings : Computation of Turbulent Boundary Layers - 1968. AFOSR-IFP-Stanford Conference, Vol. II Compiled data. Held at Stanford University, California, August 18-25, 1968
13	Haselgrove, M.K.	"Calculation of Pressure Distribution on Two Axisymmetric Boattailed Configurations". WRE Tech. Report 1779 (W), 1977
14	Albone, C.M.	"FORTRAN Programmes for Axisymmetric Potential Flow Around Closed and Semi-Infinite Bodies". ARC CP 1216, 1972
15	Landers, E.R.A.	"Unpublished Wind Tunnel Tests on a Bomb Body". WRE, 1975
16	Marsden, P.	"Results of Wind Tunnel Tests on the M823 Research Store with Fixed Monoplane Fins". ARA Model Test Note M 25/1, 1967
17	Robinson, M.L.	"Unpublished Wind Tunnel Tests on Three Axially Symmetric Configurations". WRE, 1974-1977
18	Ward, L.C.	"Force Measurements at Transonic Speeds on Axisymmetric Forebodies to Determine the Effects of Bluntness". RAE Tech. Report 76088, 1976
19	Darling, J.A.	"Handbook of Blunt-Body Aerodynamics". Vol. 1 - Static Stability. NOL Tech. Report 73-225, 1973
20	Jermey, C.	"Unpublished Wind Tunnel Tests on a Shell Configuration". WSRL, 1978

TABLE 1. COMPARISON OF MEASURED AND ESTIMATED NORMAL FORCE CURVE SLOPE AND CENTRE OF PRESSURE POSITION FOR MISSILE BODIES

Configuration	Normal force slope $-C_{Z\alpha}$			C.P. position ahead of nose (calibres)			Remarks
	Slender Body Theory	Present Method	Experiment	Slender Body Theory	Present Method	Experiment	
Body No. 1 Slender boattailed body	0.23	0.77	0.79(M_o = 0.4) 0.76 (M_o = 0.6)	37.0	7.2	8.81(M_o = 0.4) 9.39(M_o = 0.6)	$R_L = 1.9 \times 10^6$ Boundary layer trip on nose Experimental data ref.15
Body No. 2 Slender boattailed body	0.41	0.63	0.65 (M_o = 0.8)	15.8	8.6	7.60(M_o = 0.8)	$R_L = 2.2 \times 10^7$ Experimental data ref.16
Body No. 3 Non-slender boattailed body	0.26	0.57	0.63 (M_o = 0.6)	26.1	10.4	2.38(M_o = 0.6)	$R_L = 2.4 \times 10^6$ Boundary layer trip on nose Exporimental data ref.17
Body No. 4 Non-slender boattailed body with parallel afterbody	0.55	0.86	0.99 (M_o = 0.4) 0.92 (M_o = 0.6)	9.6	5.0	2.57(M_o = 0.4) 3.00(M_o = 0.6)	$R_L = 2.4 \times 10^6$ Boundary layer trip on nose Experimental data ref.17
Body No. 5 Ogive-cylinder, l/d = 6	2.00	2.11 2.23*	2.09 (M_o = 0 to 0.7)	-0.92	-1.01 -1.20*	-1.0 to -1.3 ($M_o \approx 0.6$)	$R_L = 4.9 \times 10^6$ *Rear half of afterbody treated as zero-angle boattail Normal force data ref.18 C.P. position ref.19
Body No. 6 Ogive-cylinder, l/d = 10	2.00	2.22 2.47*	2.22 (M_o = 0.4) 2.31 (M_o = 0.7)	-1.23	-1.62 -2.17*	-2.06(M_o = 0.5) -2.18(M_o = 0.7)	$R_L = 2.1 \times 10^6$ *Rear half of afterbody treated as zero-angle boattail Experimental data ref.17
Body No. 7 Ogive-cylinder with boattail	1.47	1.68	1.60 (M_o = 0.7)	0.9	-0.36	-0.36(M_o = 0.7)	$R_L = 1.8 \times 10^6$ Boundary layer trip on nose Experimental data ref.20

APPENDIX I

EVALUATION OF PERTURBATION VELOCITIES ASSOCIATED WITH NOSES, BOATTAILS AND STABILISING FLARES

The three cases illustrated in figure 1 must be examined. In each case the S"(x) distribution is zero from x = 0 until x = f, and from x = g to the end of the body at x = L. For $f \leqslant x \leqslant g$ the distribution of S"(x) varies as shown in figure 1, in each case attaining a maximum value of G.

I. Velocity distribution

I.1 Constant S"(x) distribution

For this case

$$f \leqslant x \leqslant g , \qquad S''(x) = G .$$

Inserting these values of S"(x) and S" (ξ) into equation (2) and integrating leads to the following expressions:

$$\left.\begin{aligned} &\text{For} && o \leqslant x \leqslant f \\ &&& \frac{u}{U_o} = \frac{G}{4\pi} \ln \frac{f-x}{g-x} , \\ &\text{for} && f \leqslant x \leqslant g \\ &&& \frac{u}{U_o} = \frac{G}{4\pi} \ln \frac{(\beta r)^2}{4(x-f)(g-x)} , \\ &\text{and for} && g \leqslant x \leqslant L \\ &&& \frac{u}{U_o} = -\frac{G}{4\pi} \ln \frac{x-f}{x-g} . \end{aligned}\right\} \qquad (I.1)$$

I.2 Triangular S"(x) distribution - increasing with x

For this case

$$f \leqslant x \leqslant g , \qquad S''(x) = G\left(\frac{x-f}{g-f}\right) .$$

Again, inserting these values of S"(x) and S"(ξ) into equation (2) and integrating leads to the following expressions:

For $o \leqslant x \leqslant f$

$$\frac{u}{U_o} = \frac{G}{4\pi} \left\{ -1 + \left(\frac{x-f}{g-f}\right) \ln \frac{f-x}{g-x} \right\} , \qquad (I.2)$$

$$\left.\begin{aligned} &\text{for} \qquad f \leqslant x \leqslant g \\ &\frac{u}{U_o} = \frac{G}{4\pi}\left\{ -\left(\frac{f+g-2x}{g-f}\right) + \left(\frac{x-f}{g-f}\right) \ln \frac{(\beta r)^2}{4(x-f)(g-x)} \right\}, \\ &\text{and for} \qquad g \leqslant x \leqslant L \\ &\frac{u}{U_o} = \frac{G}{4\pi}\left\{ 1 - \left(\frac{x-f}{g-f}\right) \ln \frac{x-f}{x-g} \right\}. \end{aligned}\right\} \qquad (I.2)$$

I.3 Triangular S"(x) distribution - decreasing with x

For this case

$$f \leqslant x \leqslant g \qquad S''(x) = G\left(\frac{g-x}{g-f}\right).$$

Again, inserting these values of S"(x) and S" (ξ) into equation (2) and integrating leads to the following expressions:

$$\left.\begin{aligned} &\text{For} \qquad o \leqslant x \leqslant f \\ &\frac{u}{U_o} = \frac{G}{4\pi}\left\{ 1 + \left(\frac{g-x}{g-f}\right) \ln \frac{f-x}{g-x} \right\}, \\ &\text{for} \qquad f \leqslant x \leqslant g \\ &\frac{u}{U_o} = \frac{G}{4\pi}\left\{ \frac{f+g-2x}{g-f} + \left(\frac{g-x}{g-f}\right) \ln \frac{(\beta r)^2}{4(x-f)(g-x)} \right\}, \\ &\text{and for} \qquad g \leqslant x \leqslant L \\ &\frac{u}{U_o} = \frac{G}{4\pi}\left\{ -1 + \left(\frac{x-g}{g-f}\right) \ln \frac{x-f}{x-g} \right\}. \end{aligned}\right\} \qquad (I.3)$$

II. Representation of body components

The method of employing the S"(x) distributions will now be described.

II.1 Nose (figure 8(a))

For all noses we assume that the nose length is L_N and that the body radius is r_o at $x = L_N$.

II.1.1 Conical nose

For this case

$$r = r_o \frac{x}{L_N}$$

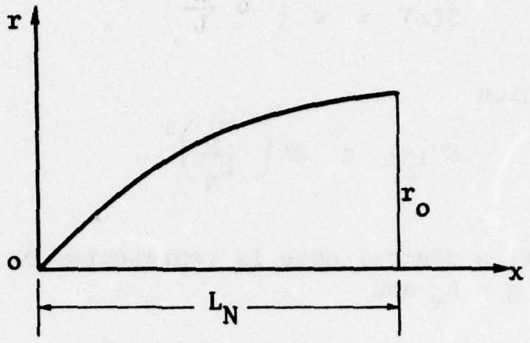

(a) Nose

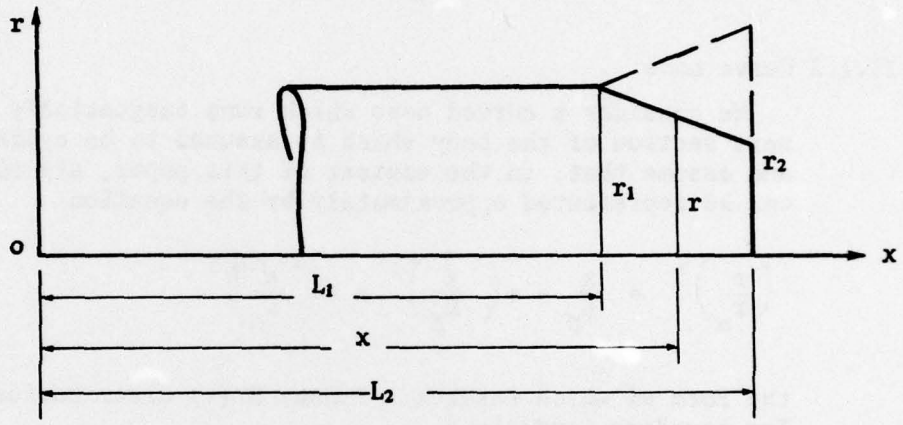

(b) Boattail or flare

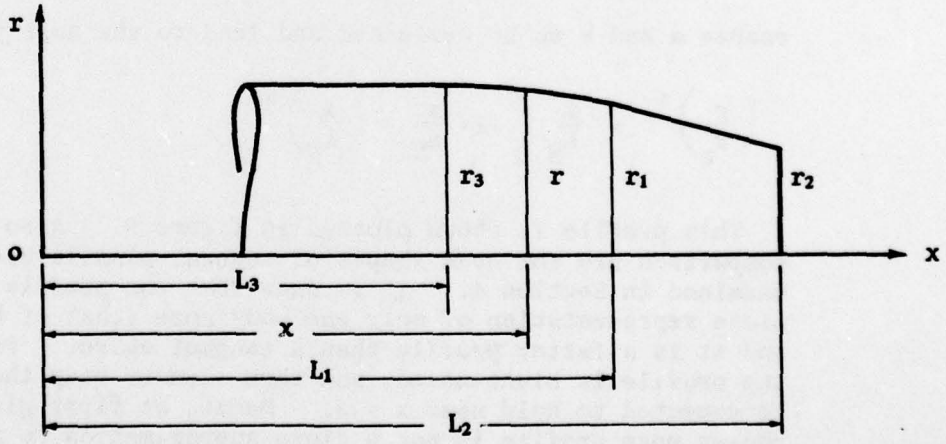

(c) Parallel section - boattail fairing

Figure 8. Body component parts

and

$$S(x) = \pi \left(r_o \frac{x}{L} \right)^2 ,$$

from which

$$S''(x) = 2\pi \left(\frac{r_o}{L_N} \right)^2 .$$

Thus, a conical nose is represented by equation (I.1) with $f = o$, $g = L_N$ and

$$G = 2\pi \left(\frac{r_o}{L_N} \right)^2 .$$

II.1.2 Curve nose

We consider a curved nose which runs tangentially into the next section of the body which is assumed to be cylindrical, and assume that, in the context of this paper, all such noses can be represented approximately by the equation

$$\left(\frac{r}{r_o} \right)^2 = \frac{x}{L_N} + a\left(\frac{x}{L_N} \right)^2 + b\left(\frac{x}{L_N} \right)^3 ,$$

the form of which ensures a linear $S''(x)$ distribution. The boundary conditions

$$x = L_N , \frac{r}{r_o} = 1, \frac{d\, r^2}{dx} = o ,$$

enable a and b to be evaluated and lead to the nose profile

$$\left(\frac{r}{r_o} \right)^2 = \frac{x}{L_N} \left\{ 1 + \frac{x}{L_N} - \left(\frac{x}{L_N} \right)^2 \right\} . \qquad (I.4)$$

This profile is shown plotted in figure 9. Also shown for comparison are the nose shapes of several missile bodies examined in Section 4. It is seen that the profile is a close representation of only one body nose (that of body no. 1) and it is a fatter profile than a tangent ogive. Furthermore, the profile is blunt-nosed, and thus slender body theory cannot be expected to hold near $x = o$. Hence, at first glance the chosen nose profile is not a close approximation to many practical nose shapes. However, this discrepancy leads to very small errors in boundary layer development because the pressure gradient is strongly favourable, and the approximation is adequate.

Equation (I.4) leads to an $S''(x)$ distribution given by

$$S''(x) = 2\pi \left(\frac{r_o}{L_N} \right)^2 - 6\pi \left(\frac{r_o}{L_N} \right)^2 \frac{x}{L_N} .$$

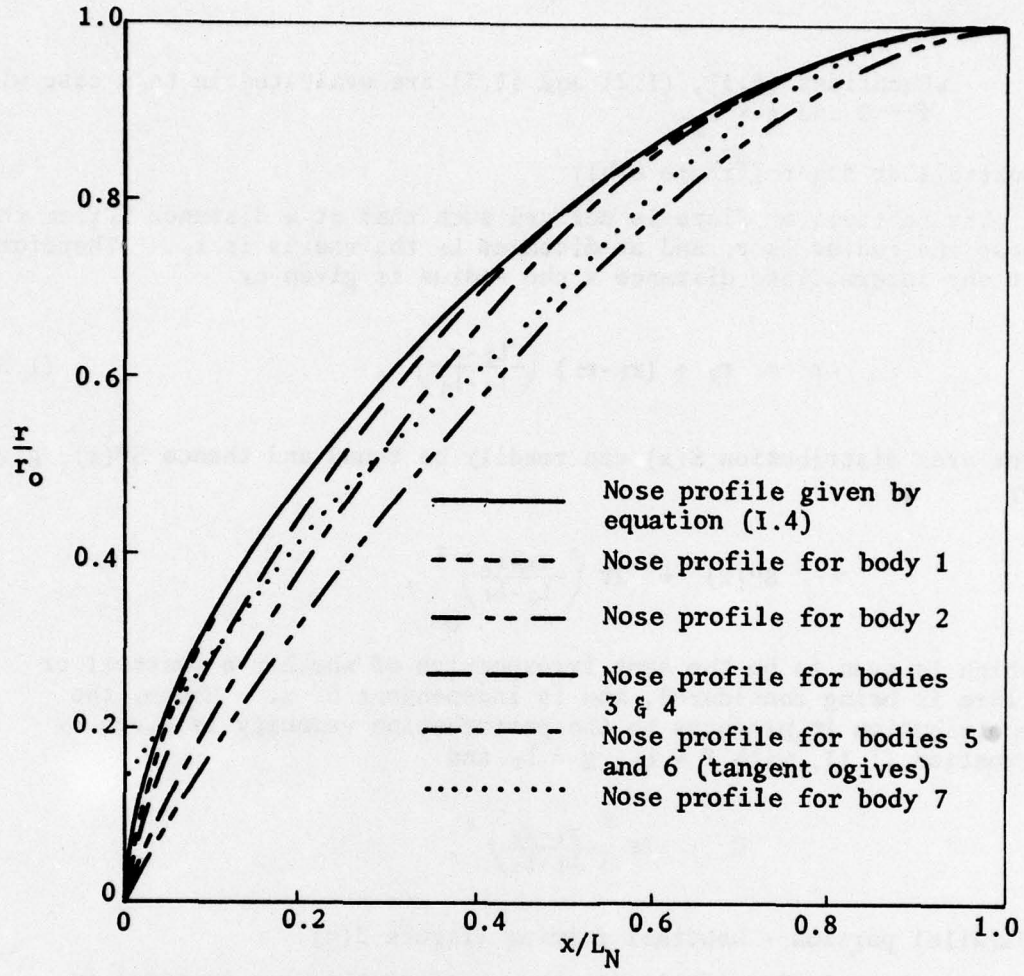

Figure 9. Comparison between nose profiles of bodies 1 to 7 and profile produced by chosen S"(x) distribution

This can be represented by the addition of two panels, namely one having constant S"(x) distribution (equation (I.1)) with $G = 2\pi\left(\frac{r_o}{L_N}\right)^2$, and one having a triangular S(x) distribution - increasing with x (equation (I.2)), with $G = -8\pi\left(\frac{r_o}{L_N}\right)^2$.

Alternatively, the representation can be by two different panels, namely one having constant S"(x) distribution (equation (I.1)), with

$$G = -6\pi\left(\frac{r_o}{L_N}\right)^2 ,$$

and one having a triangular S"(x) distribution - decreasing with x (equation (I.3)), with

$$G = 8\pi \left(\frac{r_o}{L_N}\right)^2 ,$$

Equations (I.1), (I.2) and (I.3) are evaluated in this case with $f = 0$ and $g = L_N$.

II.2 Boattail or flare (figure 8(b))

The boattail or flare is defined such that at a distance L_1 from the nose the radius is r_1 and at distance L_2 the radius is r_2. Therefore, at any intermediate distance x the radius is given by

$$r = r_2 + (r_1 - r_2)\left(\frac{L_2 - x}{L_2 - L_1}\right) . \qquad (I.5)$$

The area distribution S(x) can readily be found and thence S"(x), given by

$$S''(x) = 2\pi \left(\frac{r_1 - r_2}{L_2 - L_1}\right)^2 ,$$

which is seen to be the same irrespective of whether a boattail or flare is being considered, and is independent of x. Hence, the contribution it produces to the perturbation velocity is given by equation (I.1), with $f = L_1$, $g = L_2$ and

$$G = 2\pi \left(\frac{r_1 - r_2}{L_2 - L_1}\right)^2 .$$

II.3 Parallel portion - boattail fairing (figure 8(c))

For the majority of missile body configurations a boattail is preceded by a parallel section and the junction between the two regions can be in the form of either a sharp kink or a smooth fairing. Since the boundary layer starts to grow very rapidly downstream of this junction it is desirable to obtain a fairly close approximation to the velocity distribution here, and hence some attempt should be made to represent the fairing by an appropriate S"(x) distribution.

The fairing of length $(L_1 - L_3)$ is shown in figure 8(c). It is tangential to the parallel section at (L_3, r_3) and to the boattail at (L_1, r_1). To ensure a linear S"(x) distribution we assume that the radius squared can be represented by the cubic equation

$$r^2 = a + b\,(x - L_3) + c\,(x - L_3)^2 + d\,(x - L_3)^3 ,$$

in which the constants a, b, c and d are found by satisfying the boundary conditions

$$x = L_3 , \quad r = r_3 \text{ and } \frac{d\,r^2}{dx} = 0 ,$$

$$x = L_1 , \quad r = r_1 \text{ and } \frac{d\,r^2}{dx} = J ,$$

where J is the value of $\frac{dr^2}{dx}$ derived from equation (I.5) when $x = L_1$, namely

$$J = -2\, r_1 \left(\frac{r_1 - r_2}{L_2 - L_1} \right) .$$

Application of the boundary conditions leads to the following values for the constants:

$$a = r_3^2 ,$$

$$b = 0,$$

$$c = - \frac{1}{(L_1 - L_3)} \left\{ J + 3\left(\frac{r_3^2 - r_1^2}{L_1 - L_3} \right) \right\},$$

$$d = \frac{1}{(L_1 - L_3)^2} \left\{ J + 2\left(\frac{r_3^2 - r_1^2}{L_1 - L_3} \right) \right\} .$$

S"(x) can now be evaluated as

$$S''(x) = 2\pi \left\{ c + 3\, d\, (x - L_3) \right\} ,$$

which can be represented by the addition of two panels, namely one having a constant S"(x) distribution (equation (I.1)) with

$$G = 2\pi\, c ,$$

and one having a triangular S"(x) distribution - increasing with x (equation (I.2)), with

$$G = 6\pi\, d\, (L_1 - L_3) .$$

Alternatively, the representation can be by two different panels, one having constant S"(x) distribution (equation (I.1)) with

$$G = 2\pi \{ c + 3\, d\, (L_1 - L_3) \} ,$$

and the other having a triangular S"(x) distribution - decreasing with x (equation (I.3)), with

$$G = - 6\pi\, d\, (L_1 - L_3) .$$

Equations (I.1), (I.2) and (I.3) are evaluated with $f = L_3$ and $g = L_1$. The example dealing with body no. 1 illustrates that the representation of the fairing by the cubic in r^2 is quite accurate.

DISTRIBUTION

	Copy No.
EXTERNAL	
In United Kingdom	
Defence Scientific and Technical Representative	1 - 2
L. Pennelegion, Royal Military College of Science	3
National Lending Library of Science and Technology	4
UK National Leader, TTCP TP W-2	5 - 8
Technical Reports Centre, Orpington, Kent, BR5 3RF	9
Ministry of Defence, Defence Research Information Centre, St. Mary Cray, Orpington, Kent, BR5 3RE	10 - 15
Ministry of Defence, Procurement Executive, Castlewood House, London	
Attention: AD/TGW2	16
Aeronautical Research Council	17
Royal Aeronautical Society, Library	18
Secretary, CAARC	19
In United States of America	
Counsellor, Defence Science, Washington	20
Defence Research and Development Attache, Washington	21
US National Leader, TTCP TP W-2	22 - 25
National Technical Information Services, Springfield, Va, USA 22151	26
NASA Scientific and Technical Information Office, Washington DC, USA 20546	27
Engineering Societies Library, New York, NY, USA 10017	28
American Institute of Aeronautics and Astronautics, Library	29
Applied Mechanics Reviews	30
In Canada	
Canadian National Leader, TTCP TP W-2	31 - 34
In Australia	
Chief Defence Scientist	35
Deputy Chief Defence Scientist	36
Director, Joint Intelligence Organisation (DDSTI)	37
Superintendent, Science and Technology Programmes	38
Navy Scientific Adviser	39
Army Scientific Adviser	40

	Copy No.
Air Force Scientific Adviser	41
Superintendent, Analytical Studies	42
Defence Information Services Branch (for microfilming)	43
Defence Information Services Branch for:	
United Kingdom, Ministry of Defence, Defence Research Information Centre (DRIC)	44
United States, Department of Defense, Defense Documentation Center	45 - 56
Canada, Department of National Defence, Defence Science Information Service	57
New Zealand, Ministry of Defence	58
Australian National Library	59
BDRSS, Canberra	60
BDRSS, Salisbury	61
Superintendent, RAN Research Laboratory	62
Head, Engineering Development Establishment	63
Defence Library, Campbell Park	64
Library, Aeronautical Research Laboratories	65
Library, Materials Research Laboratories	66
Commanding Officer, Aircraft Research and Development Unit	67
Warden, RAAF Academy, Point Cook	68
Commonwealth Aircraft Corporation (Manager of Engineering)	69
Chief Design Engineer, Government Aircraft Factory	70
Library, Government Aircraft Factory	
Professor R.E. Luxton, University of Adelaide	71
Professor E.O. Tuck, University of Adelaide	
Barr Smith Library, University of Adelaide	
Australian National University, Library	72
Professor P.N. Joubert, University of Melbourne	73
Library, Engineering School, University of Melbourne	
Library, Monash University	74
Library, School of Mechanical Engineering, University of New South Wales	75
Library, University of Queensland	76
Professor G.A. Bird, University of Sydney	77
Library, University of Sydney	
Professor A.R. Oliver, University of Tasmania	78
Library, University of Tasmania	
Royal Melbourne Institute of Technology	79

	Copy No.
WITHIN DRCS	
Chief Superintendent, Weapons Systems Research Laboratory	80
Superintendent, Aeroballistics Division	81
Principal Engineer, Air Weapons Engineering	82
Senior Principal Research Scientist, Ballistics	83
Principal Officer, Aerodynamics Research Group	84
E.R.A. Landers, Aerodynamics Research Group	85
M.L. Robinson, Aerodynamics Research Group	
C. Jermey, Aerodynamics Research Group	
Principal Officer, Dynamics Group	86
Principal Officer, Flight Research Group	87
D.P. Brown, Flight Research Group	
Principal Officer, Ballistic Studies Group	88
J.S. Hunter, Ballistic Studies Group	
Principal Officer, Field Experiments Group	89
Author	90 - 93
DRCS Library	94 - 95
AD Library	96 - 97
Spares	98 - 107

The official documents produced by the Laboratories of the Defence Research Centre Salisbury are issued in one of five categories: Reports, Technical Reports, Technical Memoranda, Manuals and Specifications. The purpose of the latter two categories is self-evident, with the other three categories being used for the following purposes:

Reports	:	documents prepared for managerial purposes.
Technical Reports	:	records of scientific and technical work of a permanent value intended for other scientists and technologists working in the field.
Technical Memoranda	:	intended primarily for disseminating information within the DSTO. They are usually tentative in nature and reflect the personal views of the author.

AD-A076 128 WEAPONS SYSTEMS RESEARCH LAB ADELAIDE (AUSTRALIA) F/G 20/4
CALCULATION OF SUBSONIC NORMAL FORCE AND CENTRE OF PRESSURE POS--ETC(U)
APR 79 K D THOMSON
UNCLASSIFIED WSRL-0093-TR NL

2 OF 2
AD A076128

END
DATE FILMED
10-80
DTIC

SUPPLEMENTARY

INFORMATION

AR-001-656

DEPARTMENT OF DEFENCE

DEFENCE SCIENCE AND TECHNOLOGY ORGANISATION

WEAPONS SYSTEMS RESEARCH LABORATORY

CORRIGENDUM TO TECHNICAL REPORT

WSRL-0093-TR

CALCULATION OF SUBSONIC NORMAL FORCE AND CENTRE OF PRESSURE POSITION OF BODIES OF REVOLUTION USING A SLENDER BODY THEORY - BOUNDARY LAYER METHOD

K.D. Thomson

The following corrections should be made:

(1) On page 22 - the middle equation of (I.3) there should be a closing bracket } before the comma.

(2) On page 25 - 7 lines from the bottom, the equation should read $G = -6\pi\left(\frac{ro}{L_N}\right)^2$ in place of $-8\pi\left(\frac{ro}{L_N}\right)^2$.

(3) On page 25 - 3 lines from the bottom, the equation should read $G = -4\pi\left(\frac{ro}{L_N}\right)^2$ in place of $-6\pi\left(\frac{ro}{L_N}\right)^2$.

(4) On page 26 - top line, the equation should read $G = 6\pi\left(\frac{ro}{L_N}\right)^2$ in place of $8\pi\left(\frac{ro}{L_N}\right)^2$.

These changes do not affect any other part of the report.

POSTAL ADDRESS: Chief Superintendent, Weapons Systems Research Laboratory, Box 2151, G.P.O., Adelaide, South Australia, 5001.

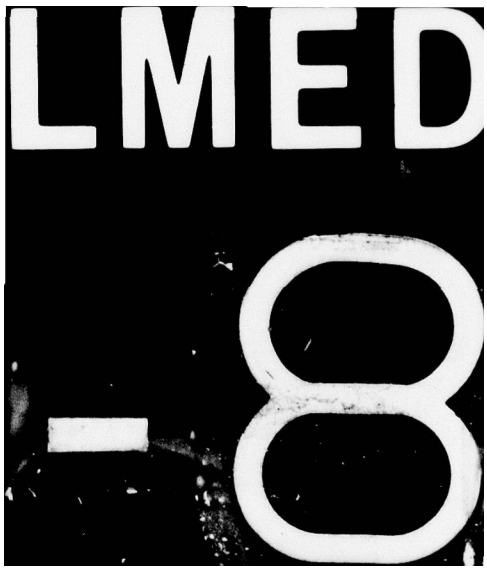
LMED
-8